Soft Matter

ARTICLE

Droplet impact on flowing liquid films with inlet forcing: the splashing regime†

Received 00th January 20xx,
Accepted 00th January 20xx

DOI: 10.1039/x0xx00000x
www.rsc.org/

Idris T. Adebayo*[a] and Omar K. Matar*[b]

The impact process of droplets falling obliquely on thin flowing films is studied using a high-speed imaging system with a focus on splashing. Frequency-forcing of the flowrate at the inlet is applied in order to form solitary waves prior to droplet impact. The outcomes associated with impact on targeted regions of the waves are examined; these include the capillary wave region preceding the large wave peak, the flat film regions, and the wave humps. The effect of varying the film flow rate, droplet size, and speed on the splashing regime for each of these regions is elucidated. The results are further compared with those associated with uncontrolled flowing films, as well as with quiescent ones. The present work demonstrates, for the first time, the contribution made by the spatial structure of waves to the outcome of droplet impact on flowing films.

I. Introduction

Droplet impact is a ubiquitous phenomenon in nature and attracts attention from any curious observer.[1] It constitutes a very important research area due to its numerous applications ranging from inkjet-printing, design of internal combustion engines, spray-cooling, spray-coating, fire-suppression, deposition of solder on bumps in printed circuit boards, surface-cleaning, and cell-printing.[2] Its application extends further to agriculture, such as in the spraying of crops as well as sprinkling irrigation.[3,4] Its study dates back to the 1900s with the pioneering work of Worthington[5] though significant advances have been made only recently due to the advent of high-speed imaging.[6]

Droplet impact has been studied on different types of surfaces ranging from solids,[7,8] shallow[9] and deep liquid pools[10,11] to thin films,[12,13] with unique phenomena observed based on the impact target. On solid surfaces, impact outcomes have been observed to lead to either bouncing, splashing or spreading depending on the wettability of the solid surface among other factors.[2,7,8] Impact on a liquid surface, however, has produced outcomes ranging from bouncing, partial coalescence, total coalescence, to splashing, [2,3,13] with the impact outcome depending on factors which characterise the physical properties of the droplet itself (such as its viscosity, density, size, etc.), the nature of the liquid surface (wavy or flat), and the conditions of impact (speed and angle).

When a liquid droplet impacts a thin film flowing down an inclined plane, the outcome of the impact will differ from that obtained on horizontal films[14] due to the oblique nature of the impact as well as contributions from the flowing film. This normally results in asymmetry of the impact outcome. However, the phenomena observed still remain qualitatively similar as mentioned above. On thin films, outcomes ranging from drop bouncing,[13,15] partial and total coalescence,[16-18] and splashing[19-22] have been studied. In bouncing, the approaching droplet is unable to merge with the liquid film, but experiences lift from the film surface.[2,13,15] This as a result of a lubrication force exerted on it by the liquid film through the intervening air layer.

With increase in the drop momentum, the resistance offered by the film is overcome and the approaching droplet is able to break the intervening air layer separating it from the film surface. This results in the coalescence of the drop with the film.[3,18] Depending on the magnitude of the drop momentum, the merger could result in the generation of a daughter droplet (usually less than a third of the mother-drop size). When this occurs, 'partial coalescence' is said to take place.[2,3,16] However, if the coalescence is complete without any product obtained from the impact, the outcome is referred to as 'total coalescence'.[3,17,18] Finally, when a droplet approaches a film surface with sufficiently high momentum that results in rupture of the intervening gas layer, a cylindrical sheet of liquid or 'corolla' is formed, which grows both radially and vertically and later disintegrates into many smaller droplets; a 'splash' is said to be observed in this case.[1-3] The key features usually studied in a splash include the 'crown' diameter, height, wall thickness, and tilt angle, as well as the number of ejected secondary droplets.[1,3,7]

The splashing event has been known to be influenced by a number of factors. One of these is the droplet Weber, which is believed to be the crucial parameter that controls splash dynamics on quiescent films.[12,14] According to Cossali *et al.,*[23] the film thickness is inversely proportional to the size of the crown formed as well as the number of secondary droplets produced. Yarin and Weiss[24] found the diameter of the ejected secondary droplets to be within a

*Department of Chemical Engineering, Imperial College London. SW7 2AZ, United Kingdom.
[a] Email: ia413@ic.ac.uk
[b] Email: o.matar@ic.ac.uk
†Electronic Supplementary Information (ESI) available:
See DOI: 10.1039/x0xx00000x

value slightly above zero and about a quarter of the primary drop diameter. According to the numerical results of Gueffier,[25] the angle of impact has a profound effect on the nature of the splashing event. Oblique impact leads to crown asymmetry with the front of the corolla being higher than at the back.

It has also been noted that for flowing liquid films, the waviness of the film surface accounts for irregularity in the shape of the ejected crown, and also for differences in the size of the secondary droplets produced.[13,14,25,26] This asymmetry occurs as a result of the oblique impact angle, while the height of the crown rim to the flow direction is often observed to be higher than that to the upstream direction, and hence more drops ejected in the downstream direction. Detailed reviews on the splash phenomena both on solid and liquid surfaces have also been carried out.[1-3,7] However, many open questions still remain, which include the origin of splashing,[26] the mechanism governing the production of secondary droplets,[3] the evolution of air layer below the impacting drop,[27] the entrapment of air bubbles[28] amongst many others.

Despite the large volume of research on droplet impact on liquid surfaces (i.e. shallow and deep pools as well as quiescent films), we observe that impact on flowing thin liquid films have not received as much attention. To the authors' best knowledge, there has been no published work on impact on films whose dynamics are influenced by inlet-forcing of the liquid flowrate; below, we refer to them as 'controlled' films. Yet this can be observed to have numerous applications in multiphase industries (e.g. in cooling towers, distillation columns, and also in the annular flow regime observed in two-phase flows), especially as film control has become an important step for the intensification of both heat and mass transfer in many process industries.[29,30]

In this paper, we present results on droplet impact on controlled flowing liquid films by the application of frequency oscillations of the inlet flow rate; this results in the formation of regular waves. We focus on the solitary wave family, which are essentially characterised by widely-separated narrow peaks, and are preceded by a series of front-running capillary waves[31-33]. We study the outcome of the impacts associated with three main parts of the solitary wave structure: the 'flat film', 'wave hump', and front-running 'capillary waves' regions. We also contrast these results with those associated with uncontrolled flowing films. Our results show that the stochastic nature of wave appearance on the uncontrolled film markedly affects the outcome of drop impact with the separate regions of the controlled film also showing new mechanisms, which we have detailed both qualitatively and quantitatively.

The rest of this paper is organised as follows. The experimental system is described in Sec. II, including the falling film rig, the film control unit, the droplet generation unit, and the high-speed imaging system. The results obtained are presented and discussed in Sec. III. We present the differences between the controlled and uncontrolled films here and give details on the effect of individual regions of a controlled film as well as the effects of key impact parameters on the impact process. Graphs of crown diameter, baseline propagation, number of secondary droplets and crown-facing direction are also plotted. Concluding remarks and suggestions for future work are provided in Sec. IV.

II. Experimental methods

A. The falling film rig

The experimental facility used in this study is shown in Fig. 1. Deionized water (density ρ = 1000 kg/m3, viscosity μ =10^{-3} Pa.s, and surface tension, σ = 72.8 mN/m) was pumped into an overhead distribution chamber; this was fitted with glass beads, which ensured the breakdown of turbulent eddies in the flow so as to obtain a uniform film beneath this chamber. The flow exited on a 57

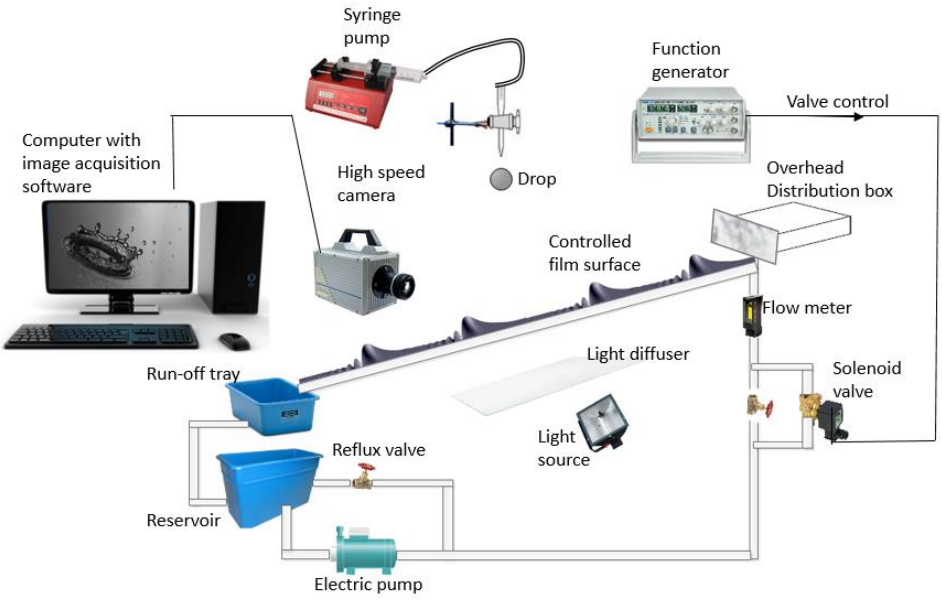

Fig. 1 Schematic of the experimental facility consisting of the falling film rig, the droplet-generation unit, the film control unit, and the high-speed imaging system.

Table 1 Physical parameters and dimensionless groups

Variable	Definition	Value/Ranges	Unit
Droplet diameter	d	0.0023 - 0.0044	m
Drop fall height	h	0.15 – 0.45	m
Droplet impact speed	v	1.7155 – 2.971	m/s
Film flowrate	q	$1.667 - 10 \times 10^{-3}$	m^3/s
Substrate inclination angle	β	15	degree
Forcing frequency	f	2-3	Hz
Fluid viscosity	μ	1.0×10^{-3}	Pa.s
Fluid density	ρ	1000	kg/m^3
Surface tension	σ	0.072	N/m
Gravitational acceleration	G	9.81	m/s^2
Nusselt film thickness	$h_N = \left(\frac{3\mu^2 Re}{\rho^2 g sin\beta}\right)^{1/3}$	$4.034 – 7.328 \times 10^{-4}$	m
Nusselt velocity	$u_N = \frac{\rho g sin\beta {h_N}^2}{3\mu}$	0.1376 – 0.4545	m/s
Film Reynolds number	$Re = \rho q/w\mu$	55-333	-
Film Weber number	$We = \rho h_N u_N^2/\sigma$	0.1061 - 2.1024	-
Drop Weber number	$We_d = \frac{\rho d v^2}{\sigma}$	94.0 – 539.4	-
Drop Ohnesorge number	$Oh = \frac{\mu}{(\rho\sigma d)^{1/2}}$	0.0018 – 0.0025	-
Kapitza number	$Ka = \sigma\rho^{1/3}/g^{1/3}\mu^{4/3}$	3363	-

cm × 30 cm glass substrate mounted on a pivot, which allowed the variation of the substrate inclination, and was collected in a run-off tray and emptied back into the reservoir tank from which the whole process was repeated continuously. The flow rate was measured by an ultrasonic flow meter (Cynergy3 UF25B, RS Components UK) connected across the flow line. The film Reynolds number, $Re = \rho q/w\mu$, was varied by changing the liquid flow rate resulting in a range of 55.5-333; with w being the channel width of dimension 0.30 m. The Kapitza number, $Ka = \sigma\rho^{1/3}/g^{1/3}\mu^{4/3}$, for de-ionised water was 3363. The ranges of all the physical parameters relevant to the present flow with the definition of h_N and u_N, which denotes the Nusselt film thickness and velocity, respectively, are detailed in Table 1.

B. Film control unit

A function generator (GW INSTEK AFG-205 series Digital) was used to automate the control of a solenoid valve (SMC VXD series-pilot-operated-two-port), connected via a non-latching relay (Takamisawa A5W-K) and a by-pass. The solenoid valve was connected to the primary circuit downstream from the flow rate control valve, and in addition to a bypass around it. The purpose of the bypass was to ensure that film flow is sparsely maintained on the substrate even when the solenoid valve is short. A ball valve is used to control the amount of flow through the by-pass, while the solenoid valve itself is made to receive wave signals from a data acquisition card (National Instrument DAQ, UK) via a non-latching relay (Takamisawa A5W-K). Signals from the function generator were simply communicated to the DAQ card. Different parameters on the output signal including frequency and wave type (sine wave, saw tooth wave to a square wave etc.) were selected as desired while the output signal was simply translated into the opening and closing of the valve by the relay. A forcing frequency of 2-3 Hz was used in this study to facilitate a clear demarcation between the regions of the controlled film surface.

C. Droplet generation unit

A syringe pump (Briantree Scientific Inc. UK) was used to pump de-ionized water through a plastic tubing to a blunted syringe needle. Different sizes of the syringe needles were used to vary the diameter of drop produced. The flow rate of the liquid entering the syringe was set and uniform sized drops produced. The syringe needle was held above the film at desired calculated heights above the film surface.

The drops broke from the tip of the syringe in a 'dripping' mode and fell under their own weight without prior acceleration. They impacted obliquely on the film surface, 30 cm from the film inlet. The range of drop diameter, *d*, studied were between 2.3 – 4.4 mm while the corresponding Ohnesorge numbers, *Oh*, were between 0.0018 – 0.0025. The physical properties of the drop are the same as those of the film. The impact speeds were varied by changing the height from which the drops fell, from 15 cm to 45 cm, giving drop speeds between 1.7155 – 2.971 m/s with corresponding Weber numbers, We_d, between 94.0 – 539.4.

D. High-speed imaging system

An Olympus i-SPEED 3 camera was used for high-speed imaging in conjunction with two separate lenses: Nikon AF Micro-Nikkor 60 mm f/2.8 D lens, and a Sigma 105mm f/2.8 Macro Ex lens. The former and latter were used to take top- and side-view images of the process, respectively. For the top-view images, the camera was placed in the wall-normal direction to ensure a sharp focus of the film surface is achieved. A central position was also maintained in the spanwise direction, to minimise potential boundary effects from the substrate edges. For the side-view images, deviations of 7˚ and 12˚ to the film surface (horizontally) and flow directions, respectively, were maintained in order to obtain the best possible view of the impact process; giving a pixel size of 67.5µm/pixel and 46.6 µm/pixel in the streamwise and spanwise directions, respectively. In both cases, the camera was used at a frame rate of 5000 frames per second, 800×600 resolution, aperture size 16 and a shutter speed of 1 ms. The computer control unit facilitated the triggering of snapshots, which were set to capture the most desired instances on the camera shot. Illumination was achieved by means of halogen lamps used with a diffuser below the glass substrate. These were chosen specifically since they did not produce flickers at high recording speeds. The high-speed images acquired were then analysed using a customised *Matlab* programme from which videos of the flows, and quantitative information were extracted. Due to free-surface oscillations usually experienced by droplets falling in a dripping mode, the near-impact images were carefully checked to ensure the drops still retained their spherical shape before impact.

III. Results and discussion

A. Film control

We commence this section by giving a short overview of the nature of wave evolution on an 'uncontrolled' film (i.e. in the absence of inlet-forcing of the flowrate). Beyond the critical Reynolds number for wave evolution on a film surface, $Re_c = {}^5/_4 \cot\beta$[34], calculated as 4.67 here for the inclination angle examined i.e. 15˚, natural waves are always observed to form on a flowing film. These waves appear as a result of the amplification of the infinitesimal disturbances from random noise at the inlet that trigger the evolution of long waves on the film surface.[31,35] The result of this primary instability is first observed in the form of two-dimensional periodic waves, seen near the inlet, which develop downstream into solitary waves preceded by a series of front-running capillary ripples.[29,31,32] These two-dimensional solitary waves transition downstream into three-dimensional ones to form "horseshoe" structures.[31-33] The natural development of these waveform takes a considerably long streamwise length scale to be observed[29,35], and is often punctuated by spatio-temporally-irregular dynamics.[31,32]

To obtain waves that have spatio-temporally-regular dynamics, periodic inlet forcing of the liquid flowrate is necessary.[29,35] A number of studies have been carried out in this area,[30-35] and the results confirm the effectiveness of the forcing in giving rise to regular waves. Depending on the characteristics of the forcing applied, two families of waves have been noted in the literature:[32,35] the so-called γ_1 and γ_2 waves. The latter are obtained at low forcing frequencies, and are characterised by widely-separated narrow peaks, which are preceded by a series of front-running bow waves.

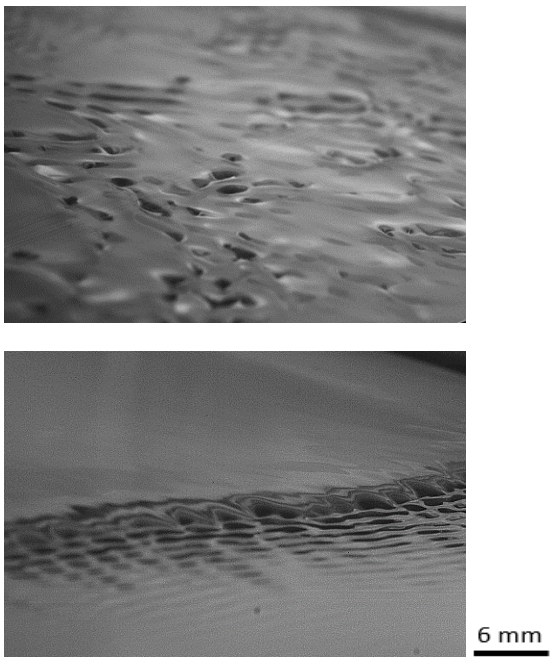

Fig. 2 Effect of film control on wave evolution on a flowing liquid film. (A) Shadowgraph image of naturally evolving waves on a liquid film (B) Shadowgraph image of forced waves on a controlled liquid film.

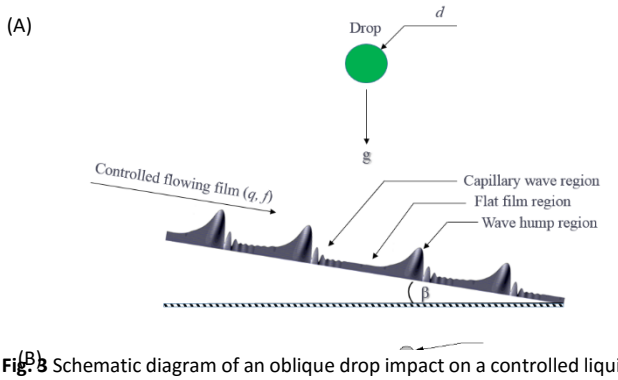

Fig. 3 Schematic diagram of an oblique drop impact on a controlled liquid film. The individual regions on the film have been highlighted for easy identification, namely the 'capillary wave', 'flat film', and 'wave hump' regions. Fig. A corresponds to an unscaled representation of the impact while Fig. (B) shows approximate length scales of the individual regions.

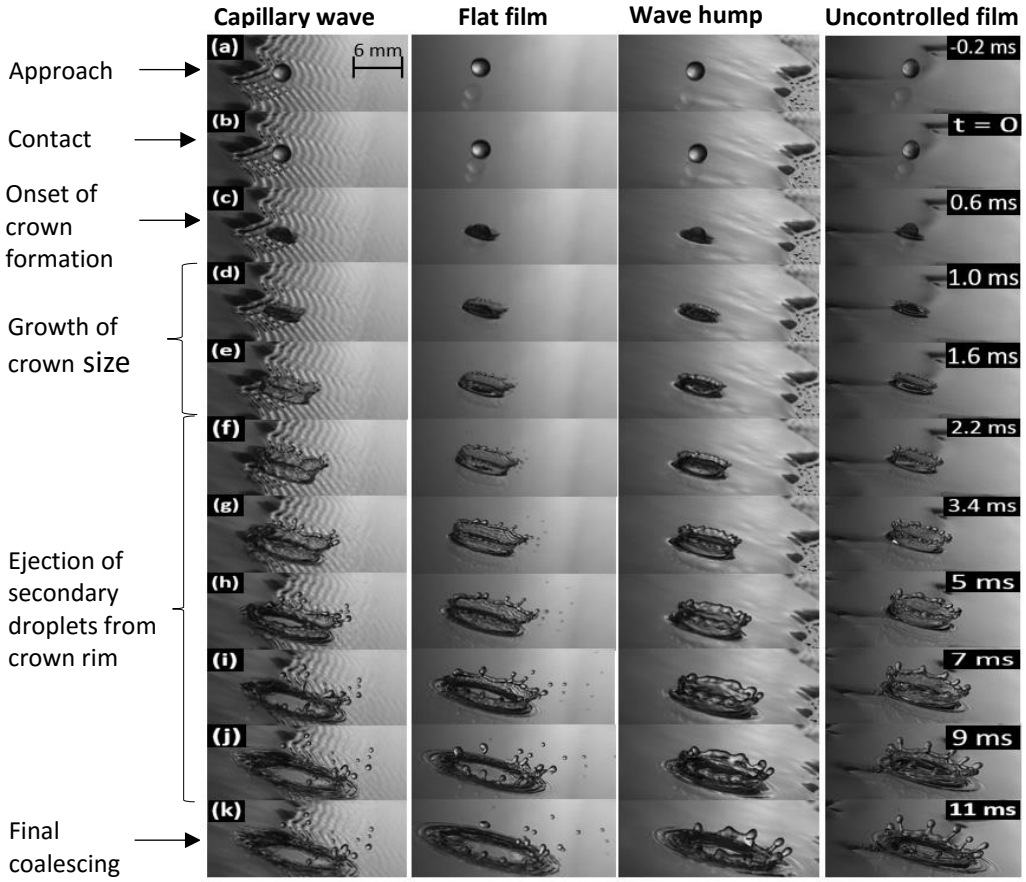

Fig. 4 Splashing phenomena on the different regions of impact on a controlled flowing film identified in Fig. 3, contrasted against an uncontrolled film. The droplet diameter is 0.0033 m, with a fall height of 25 cm while the film flow rate is 5×10^{-3} m³/s, corresponding to *Oh* = 0.0021, We_d = 224.8, and film *Re* = 166.5, respectively. Forcing was carried out at 2Hz. The liquid drop approaches the film surface (a) and immediately upon contact (b), develops an ejecta sheet which grows into a crown (c). The growing crown (d-e) later yields to a Rayleigh-Plateau instability which leads to the ejection of smaller droplets from its rim (f-j). The crown collapses afterwards and coalesces with the film (k), being transported away by the oncoming flow. The unique differences in the impact outcome on the individual regions of impact are seen in the size (height and diameter) of the crown formed, number of ejected secondary drops degree of crown tilt, crown facing direction and final coalescence time.

The former are sinusoidal-like waves observed at high forcing frequencies, and characterised by large singly and closely-peaked crests. The effect of film control on wave evolution is shown in Fig. 2

In this study, we consider three distinct regions along the wave. The first region, as shown in Fig. 3, is the 'capillary wave region'. This corresponds to the series of front-running capillary waves that preceed a developed solitary waveform. The second is the 'flat film region', which corresponds to an essentially waveless portion of the film surface that is the tail that follows a solitary waveform. Finally, the last observable region on the film surface is a 'wave hump region' which corresponds to the crest of a solitary wave hump, and is thicker than the average film surface.[31,32,35] All of these regions are exploited to examine their unique effect on drop impact dynamics.

B. Typical phenomena, and effect of film control

We commence the presentation of our results by contrasting the impact of a single drop on an 'uncontrolled' film with that on the different regions of a 'controlled' film, for the same drop size, speed, and film flowrate; this is shown in Fig. 4 for We_d = 224.8, *Re* = 166.5, and *Oh* = 0.0021; the corresponding top-view images are shown in

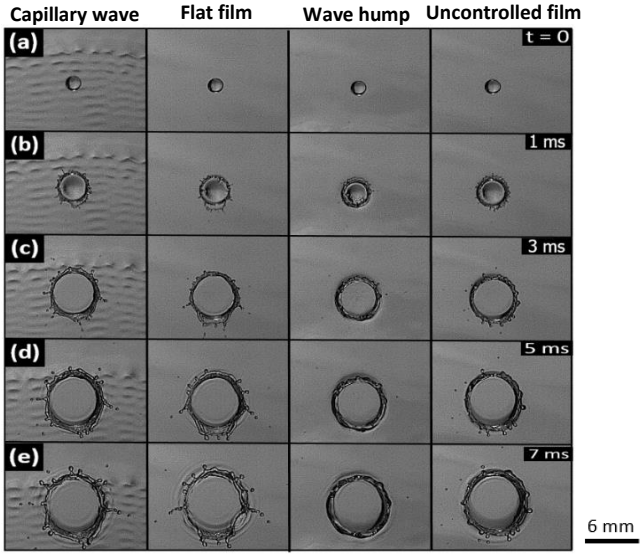

Fig. 5 Top view shadowgraphic images showing drop impact process on a controlled flowing film contrasted against an uncontrolled film. The images are arranged in columns associated with the 'capillary wave', 'flat film', 'wave hump' regions, and uncontrolled film, from left to right, respectively. The parameters correspond to those used to generate Fig. 4.

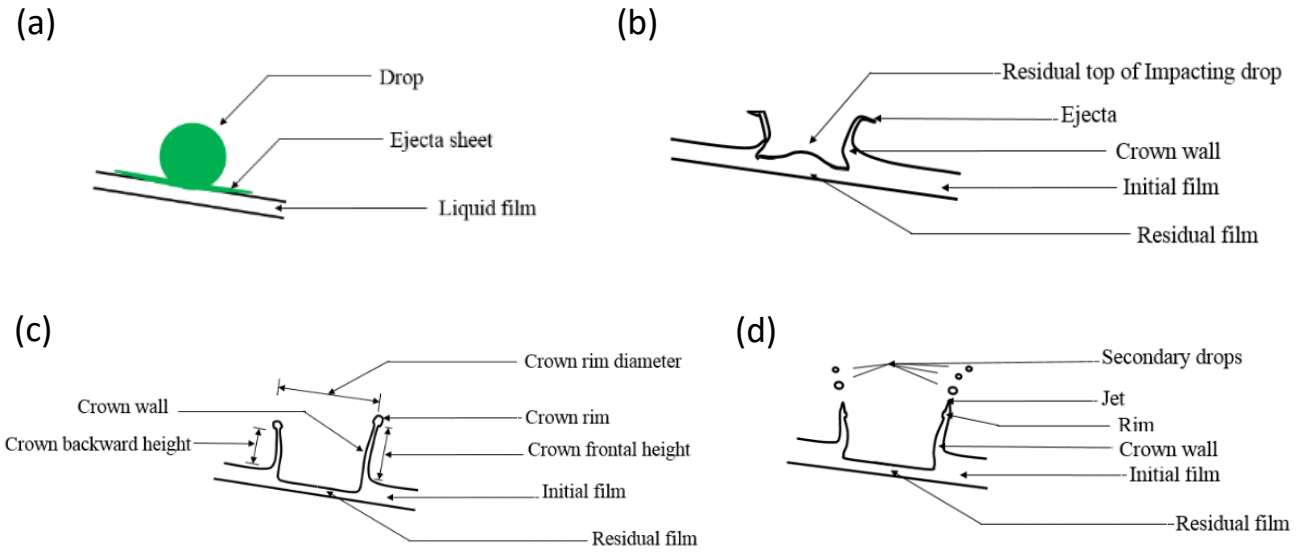

Fig. 6 Schematic diagram of the impact process of a drop obliquely impacting a thin liquid film. The individual stages are (a) Ejecta formation (b) Crown evolution (c) Crown formation (without secondry drop) (d) Secondary drop generation on a Crown. Due to the oblique nature of the impact as well as the effect of liquid film flow, assymetry in crown structure is observed which in turn affects the direction to which more secondary drops are ejected.

Fig. 5. The droplet approaches the interface (Fig. 4a), and touches the film at time, t = 0 (Fig 4b). After the droplet impinges on the film, an ejecta sheet of liquid is formed around the droplet (Fig. 4c), which grows into a crown shape (Fig. 4d-f). The rim of this crown then undergoes a Rayleigh-Plateau instability, which leads to smaller, secondary droplets being ejected (Fig. 4f-j). Afterwards, the crown collapses and coalesces, flowing away with the oncoming flowing liquid film (Fig. 4k).

The phenomena described above agree with those in the literature on the splash outcome dynamics[1,2,3] as also shown in the schematic illustration of the physical mechanisms depicted in Fig. 6. Nevertheless, differences exist between the distinct film regions in terms of crown size (height and diameter), number of secondary droplets and coalescence time. Due to the stochasticity of the wave dynamics on uncontrolled films, impact outcomes are also stochastic in nature, and their results are presented in a statistical sense.[13,14] On controlled films, however, these outcomes are reproducible, and possess unique dynamics.

In the 'wave hump region', the crown structure is different from that in the 'capillary' and 'flat film regions': its shape is more regular (see Fig. 4d-f; column 3). It also possesses a thicker crown wall (see Fig. 4g, h; column 3), and the crown height is higher than those observed in the 'capillary' and 'flat film regions' (see Fig 4h, i; column 3). There are also fewer secondary droplets ejected from its rim in comparison with the crowns formed in the other regions (see Fig. 4i - k; column 3). Finally, a longer coalescence time (see Fig. 4k; column 3) is observed before the crown is swept away by the flowing film. These observations on the wave hump reveal quite subtle uniqueness of this region of the controlled film. While the increased liquid mass in this region differentiates it from other regions, studies in the literature have shown that the flow field beneath reveals a different behaviour from those in the flat film and capillary wave regions. Craster and Matar[29], Kalliadasis *et al.*[35], and Charogiannis *et al.*[36] have shown that solitary wave usually exhibits a separation of scales between the front of the wave hump and the tail, which is characterised by a balance of gravity, viscous drag, and surface tension. This has been found to lead to a strongly non-parabolic velocity profile at the wave front, with a recirculation zone observed in the wave hump and flow reversal in the capillary wave region (Fig. 7). Contributions also from the high film velocity experienced at the wave hump[37] compared to the other regions also add up to the reasons behind the change in the dynamics of the impact outcome.

In the 'capillary wave' and 'flat film region' (images in the first and second columns, respectively), the crowns formed are also quite different based on a number of features. First, it was observed that the rear height of the crown is affected by the capillary humps as well as the flow reversal dynamics in this 'capillary wave region', hence causing the crown formed to appear more upright. This flow reversal results in the transport of liquid mass backwards which augments the rear height of the crown formed. This, however, is not observed on the flat films: the crown is naturally tilted in the liquid flow direction

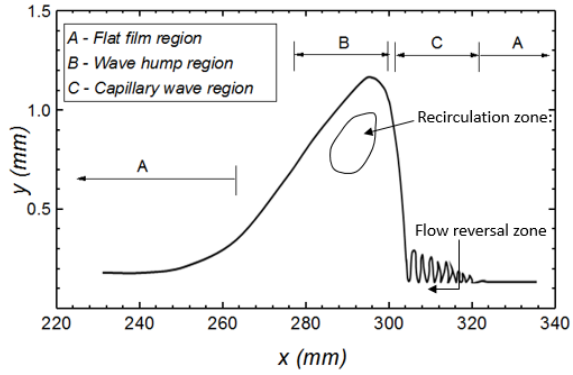

Fig. 7: Flow profile in a typical solitary wave structure. The individual zones of recirculation (i.e. in the wave hump) and the flow reversal zone in the capillary wave region have been indicated for easy identification.

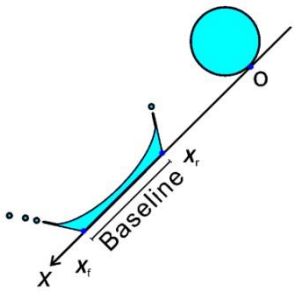

Fig. 8 Droplet baseline propagation on a flowing liquid film. The origin denoted the point of impact on the film surface while the streamwise direction is defined as the positive direction for both the front and rear points.

and tilts even further with increasing *Re*. This tilt can be observed in both the upstream and downstream ends of the crown. The implication of these observations on the crown baseline evolution is studied in more detail in Sec. IIIC.

In comparison with the capillary waves, as the film *Re* is increased, the rear side of the crown appears to become more 'upright' in a manner quite opposite to that observed on flat films. The crown height on the flat film is also higher than that on the capillary waves due to the confinement of the substrate (Fig. 4e, f). There is also a more rapid onset of secondary droplet ejection from the crown rim, on the flat films in comparison with that on capillary waves (see Fig. 4g, h). Finally, more secondary droplets are ejected on the rim of the crown on flat films than that on capillary waves (See Fig. 5i, j). The phenomena discussed above are studied in more detail in the next section, and the physics of the impact process is also carefully examined.

C. Effect of system parameters on droplet impact

To understand the physics underlying the phenomena reported in the previous section, a number of physical parameters were varied and their respective effect on the crown features studied quantitatively; these included the drop speed, film flow rate, and the drop size, which culminated in the variation of We_d, *Re*, and *Oh*. The crown features studied also include the diameter, baseline propagation, and number of ejected secondary droplets. For the baseline propagation, as shown in Fig. 8, we assume the drop impacts the film surface at a point, denoted in the results presented in Figs. 9-11 as the 'origin'; we also adopt the convention that the streamwise direction downstream of the origin is positive. We further normalize the length of the drop baseline as well as the front and rear points, x_f and x_r, by the drop diameter (see Fig. 8), while time is normalized by the drop diameter divided by its speed.

- **Film Reynolds number**

Figure 9 shows the effect of varying *Re* on the outcome of drop impact in the different regions of a controlled film. The parameters used correspond to We_d = 224.8, *Oh* = 0.0021, (with drop fall height 0.25 m and diameter 0.0033 m) while the *Re* values are 55.5, 166.5, and 310. As can be seen from Fig. 9(a), the temporal evolution of the crown diameter is weakly-dependent on *Re* in all regions of the flow. The weakest dependence on *Re* is observed in the 'wave hump region', where all the curves associated with these regions exhibit significant collapse. These observation confirm the findings of Reiber *et al.*[38] that the film Reynolds number does not tangibly affect the evolution of the crown diameter.

In Fig. 9(b), which depicts shadowgraphic plots of the splash associated with each region, shown parametrically for different *Re* values, a number of observations can be made. In the 'flat film region', the crown height is observed to increase with *Re* in the 'flat film region', as expected, since larger *Re* are associated with thicker films. Roisman and Tropea[39] confirmed this also in their studies on static films with varying film thickness. The degree of crown inclination towards the flow direction is also higher with increasing

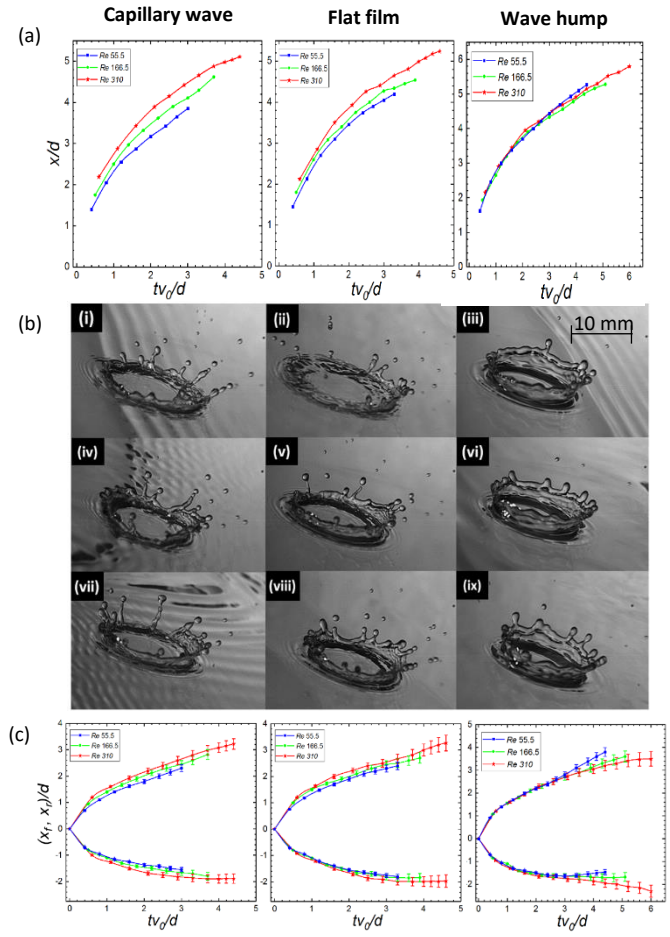

Fig. 9 Effect of film flow rate on the splashing phenomena. (a) Temporal crown diameter evolution; (b) snapshots of the crown formed 7 ms after the impact; (c) evolution of the crown baseline for the different regions of impact. The droplet fall height is 0.25 m and the drop diameter is 0.0033 m corresponding to We_d = 224.8 and *Oh* = 0.0021. The film flow rates are 1.66, 5, and 9.3×10^{-3} m³/s corresponding to *Re* = 55.5, 166.5, and 310, respectively; forcing was carried out at 2Hz. Images are arranged as 'capillary wave', 'flat film', and 'wave hump regions', from left to right, respectively.

Re in the 'flat film', and 'wave hump' regions; this effect, however, appears to be less pronounced in the 'capillary wave region'.

In the 'wave hump region', there are fewer secondary droplets ejected with increasing *Re* which may be due to the absorbing effect of the liquid mass in the wave hump on the inertia of the approaching drop which then in turn stabilises the crown formed against the Rayleigh Taylor instability. There appears to be a somewhat weak dependence of the crown height on *Re*, while there is a decrease in the crown coalescing time (not shown) with increasing *Re* which is the result of the increased speed of the flowing film upon which the impact occurs, which quickly sweeps the coalescing crown away from the original impact point. In the 'capillary wave region', more

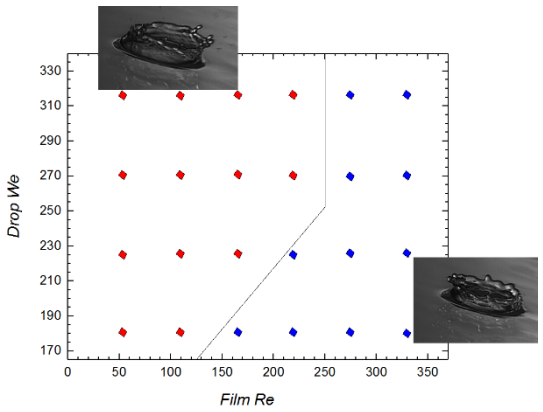

Fig. 11 Effect of film Reynolds and drop Weber on crown propagation in the 'wave hump region'. The droplet size is 0.0033 mm corresponding to *Oh* = 0.0021 and the drop fall heights has been varied from 0.20 – 0.35 m (corresponding to We_d = 179.8 – 314.7) while *Re* is in the range of 55.5 – 333. The red diamonds depict outcomes with the crown facing the downstream direction while the blue diamonds show upstream-facing crown outcomes.

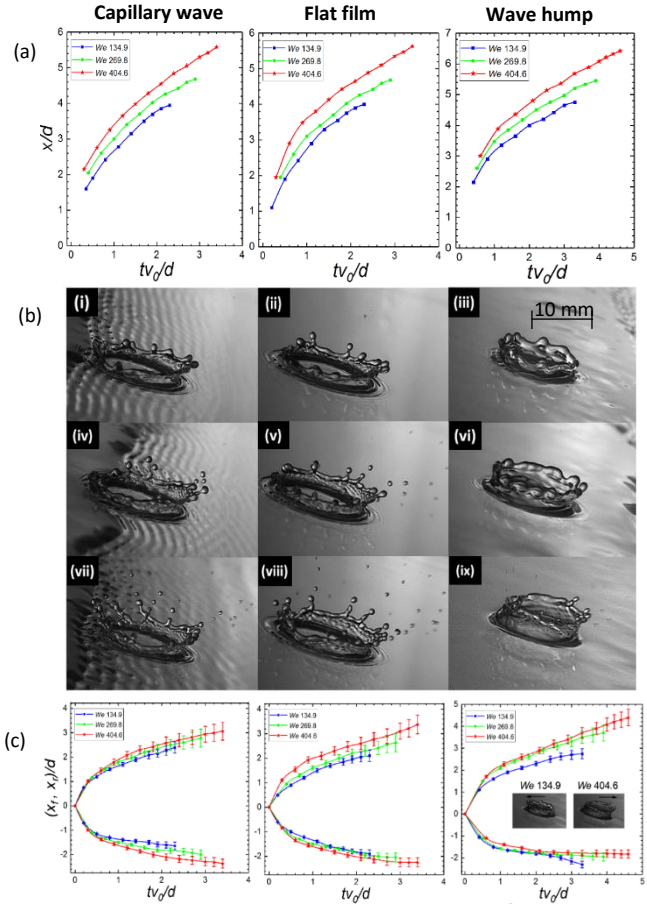

Fig. 10 Effect of drop Weber number on the splashing phenomena. (a) Graphs of temporal crown diameter evolution; (b) snapshots of the crown formed 7 ms after the impact; (c) evolution of the crown baseline on the different regions of impact. The diameter of impacting drop is 0.003 (corresponding to *Oh* = 0.0021) while the film flowrate is 6.67×10^{-3} m³/s (corresponding to *Re* = 222). The droplets fall-heights are 0.15, 0.3 and 0.45 respectively (corresponding to We_d = 134.9, 269.8, and 404.6) and forcing was carried out at 2Hz. Images are arranged as 'capillary wave', 'flat film', and 'wave hump regions', from left to right, respectively. The splash images in panel (c) associated with the 'wave hump region' are for *We* = 134.9 and 404.6.

secondary droplets are observed at lower *Re* (see Fig. 9(b), first column). There is also an increase in the overall crown height with *Re*, and, at lower *Re*, droplet ejection is mainly towards the streamwise direction (with the crown rim higher at the front than at the rear [in the sense of Fig. 8] and also tilted more towards the streamwise direction). The height becomes more symmetric at higher *Re* (more visible in the movies available online). This is an interesting phenomenon and it is most likely to be as a result of the balancing effect of the higher humps which capillary waves possess at their rear, thereby balancing-off the crown rim height at the back.

In Fig. 9(c), the propagation of the crown baseline is shown. In general, it can be observed that both front and rear points of the baseline propagate faster with increasing *Re* (see Fig. 9(c), first and second columns), due to the more rapidly-moving films. In the 'wave hump region', it can be seen that at the lowest *Re* values investigated x_r initially moves upstream of the point of impact, then reverses its direction of motion. This gives way to a situation wherein the baseline rear travels monotonically upstream of impact with increasing *Re*. The increase in *Re* also leads to a decrease in the rate of downstream propagation rate of x_l. These results demonstrate the different effect of the film flow rate on the impact dynamics associated with the various regions along the wave and also confirms predictions from Mitchell *et al.*[40] and Hann *et al.*[41] that static film models cannot not be fully used for flowing liquid films. The reader is, nonetheless, referred to Hobbs and Osheroff[9] and Hann *et al.*[41] for an overview of impact on films with sufficiently large film thicknesses relative to the drop diameter.

- **Drop Weber number**

Figure 10 shows the effect of We_d on the splashing phenomena on a controlled flowing film. The parameters used correspond to *Re* = 222, *Oh* = 0.0021, and the We_d values are 134.9, 269.8, and 404.6. From Fig. 11(a), it can be observed that the crown diameter increases at a greater rate with increasing We_d; the largest rate is associated with the 'wave hump region'. As seen in Fig. 10(b), there is a change in the

inclination of the crown in the 'wave hump region' depending on the value of We_d. At the lower We_d investigated, the crown faces the upstream direction, while at the higher We_d values, it faces downstream (see Fig. 10(b), third column). This trend is not observed in the 'capillary wave' and 'flat film regions'.

The crown inclination is important because it dictates the direction to which more secondary droplets are ejected. This, in turn, is significant particularly with regard to many types of process equipment in which droplet splashing is a major factor in its operation[2,3]. To elucidate the dependence of the crown inclination on system parameters, a plot of We_d vs. *Re* is shown in Fig. 11 for *Oh* = 0.0021, *Re* = 55.5–333, and We_d = 179.8–314.7. From this figure, it can be observed that the crown inclination is affected by the competition between the inertia of the impacting drop and that of the flowing film. It is noted specifically that at low *Re*, the crown is inclined towards the streamwise direction. As the inertia of the flowing film gains in importance, however, the direction of the crown changes and faces upstream. We have found that the crown inclination maintains a upstream-facing direction beyond a *Re* value of approximately 250 regardless of the magnitude of We_d.

It is also observed that at high We_d, few drops are ejected from the free rim of the crown in the 'wave hump region' while none are ejected on the crowns at the lower We_d studied (see Fig. 10(b), third column). This is due to the reduced inertia of low We_d drops which makes the crowns formed more stable. The crown height also increases with We_d, while the crown coalescence time increases with We_d due to its increased liquid mass. This is in agreement with the findings of Mitchell *et al.*[40] and Cossali *et al.*[42] that increasing drop Weber always increase the collapse time of a cavity. In the 'capillary wave region', however, different dynamics are observed. First, there is an earlier onset of secondary droplet ejection with increase We_d, resulting from the unstable nature of crowns formed here; as well as the ejection of more secondary droplets (see Fig. 10b-i,iv,vii) which is in agreement with previous findings in the literature[1,2,3]. However, we note that the size distribution of the impact products become smaller (see Fig 10b-vii and Fig 14). The secondary droplet area of ejection also increases with *We,* which can be attributed to the effect of the drop increased inertia and contributions from the reversing flow leading to more area on the crown rim yielding to the Rayleigh-Plateau instability.

With increase in We_d on the flat film region, there is also an earlier onset and a more frequent ejection of secondary droplets (see Fig. 10b-ii,v,viii). This can be attributed to the fact that the rim of the crown formed at a higher We_d tends to yield easily to Rayleigh-Plateau instability, hence ejecting secondary droplets quicker,[1,2] while the crown on the wave hump is more stable to it.

In Fig. 10c, it can be observed that the front points of the crown baseline travel faster than the rear points on all the impact regions due to the oblique nature of the impact and the inclination of the glass substrate. However, a number of striking features are evident, which show clear differences. On the wave hump, it can be noticed that as the drop We_d is increased, the rear point of the crown changes direction (facing backwards) (see column 3, Fig 10c). This change of direction has been observed in the shadowgraphic images earlier and are inset in this plot for easy identification. This is however, not observed on other regions of the film surface. On the flat film surface, both the front and rear points of the crown baseline travel faster as We_d is increased but the front propagates much faster than the rear in each separate case. This front point leaning more forward is also observed in the shadowgraphic images as a sharper tilting of the crown in the streamwise direction when the We_d value is increased.

On the Capillary wave region, both front and rear points are also observed to travel faster with increase in drop We_d. However, there

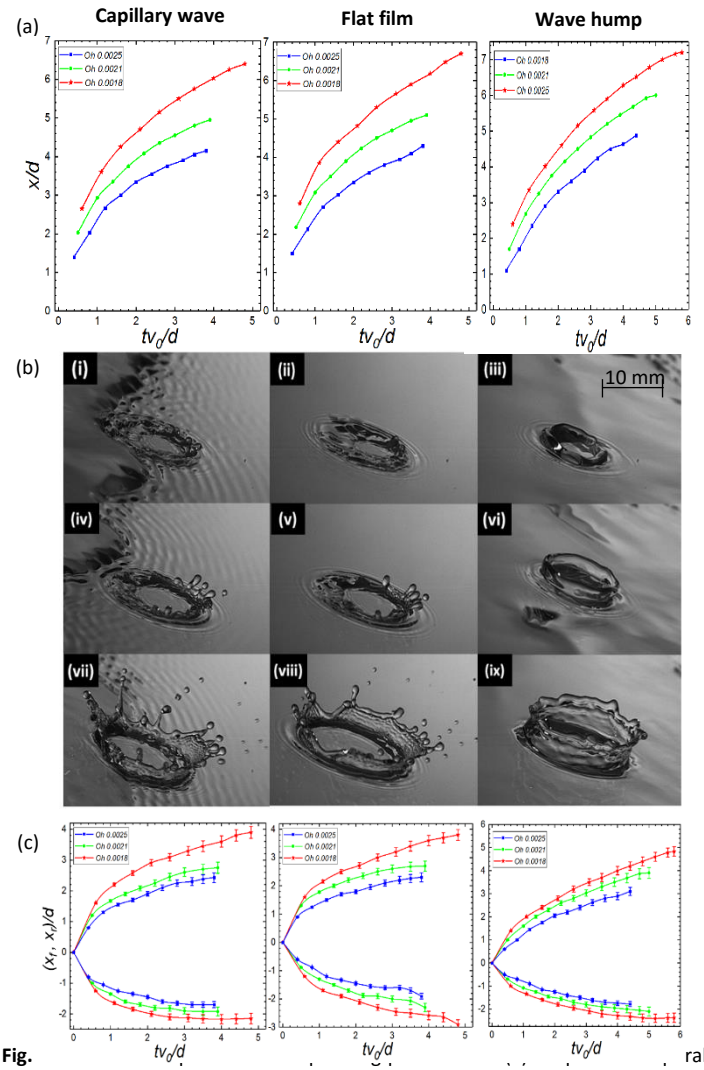

Fig. ral crown diameter evolution; (b) snapshots of the crown formed 7 ms after the impact; (c) evolution of the crown baseline on the different regions of impact. The fall height of the impacting drop is 0.25 m (corresponding to We_d = 224.8) while the film flowrate is 6.67 × 10^{-3} m^3/s (corresponding to *Re* = 222). The droplets diameters are 0.0023, 0.0033 and 0.0044 (corresponding to *Oh* = 0.0025, 0.0021 and 0.0018, respectively). Film forcing was carried out at 2Hz. Images are arranged as 'capillary wave', 'flat film', and 'wave hump regions', from left to right, respectively.

is a balancing up of the crown baseline structure as We_d number is increased. This is seen in the even spacing observed between the front and rear point propagation lines. Hence, in summary, the crown evolves uniquely and differently on these regions of impact.

- **Drop Ohnesorge number**

Figure 12 shows the effect of drop size on the splashing phenomena on a controlled flowing film. The parameters used correspond to *Re* = 222, We_d = 224.8, and *Oh* = 0.0025, 0.0021 and 0.0018. From the plots of crown temporal evolution (Fig. 12a), we observe that there is a noticeable increase in the crown diameter with decreasing *Oh*, which corresponds to increasing drop diameter. This effect is discernible in all impact regions, and is particularly accentuated at the wave hump and can be clearly seen in the shadowgraphic images shown in Fig. 12b. The increase in crown diameter with drop diameter occurs due to the increased inertia of larger impacting drops, which results in larger crowns being formed. This also agrees with previous findings in the literature.[1,2,13]

From the images in Fig. 12(b), we also observe that for the smallest droplets studied, there are no secondary droplets ejected after impact (see Fig.12b- i,ii,iii). The crown/ring formed simply coalesces and is carried away by the oncoming liquid film flow. This occurs due to the reduced kinetic energy of the impacting drop which makes the crown small and less vulnerable to instability. However, with increase in the droplet size, the crown becomes less stable and this results in the generation of daughter droplet from the crown rim, with the highest number of droplets generated by the largest drop (see Fig. 12b-vii,viii,ix). In comparison however, fewer drops are generated on the wave hump while a higher value is recorded on the 'flat film region'. A detailed discussion on the effect of both film *Re* and drop We_d on the number and size distribution of secondary droplet is given in Sec.IV.

In terms of the crown structure, the crown height is observed also to increase with decreasing *Oh* (i.e. increasing drop size) (see Fig. 12b- vii,viii,ix) which occurs as a result of the increased liquid mass introduced to the film by larger drops. This confirms the predictions by Che *et al.*[13] that the crown height is an increasing function of the initial drop diameter. Finally, it can be observed as well that the coalescing time for the developed crown increases with drop size due to the increased resistance offered by the larger crowns formed.

From Fig. 12c, we observe that the front and rear points of the crown baseline generally propagate faster as the drop size is increased. This is observed in all the regions of impact. The rate of propagation of the front point, however, is always higher that the rear. This is believed to be a result of the oblique nature of the impact and aided by the flow of the liquid film. This propagation is also observed to be highest on the wave hump in comparison with the other two regions. On the capillary wave region, the rear point is generally observed to extend further backwards in comparison with the flat film and the wave hump region. This backward motion is believed to be a result of the flow reversal occurring in this region as well as the balancing effect caused by the capillary ripples.

D. Scale relationship for crown evolution

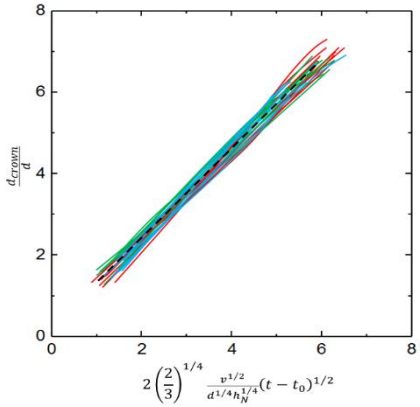

Fig. 13 Crown diameter evolution (initially plotted in Figs. 9a, 10a and 12a); now scaled using the scaling relationship of Yarin and Wess[43]. The curves collapse into a straight line with a gradient of$\vartheta = 1.23$ (black dashed lines). The red curves depicts impact on the wave hump, the green curves, the flat film and the blue curves the capillary wave region respectively.

From the analysis above, the crown propagation is a function of system parameters which include the drop impact speed, size, and film flowrate. To further quantify the cumulative effect of these parameters on the impact process, we have provided a scaling relationship for the crown propagation, following the initial scaling proposed by Yarin and Wess[43].

$$\frac{d_{crown}}{d} = 2\left(\frac{2}{3}\right)^{1/4}\frac{v^{1/2}}{d^{1/4}h^{1/4}}(t-t_0)^{1/2}, \quad (1)$$

where t_0 is the shifted time, which is obtained by fitting of the experimental data. In Fig. 13, we have plotted the dimensionless crown rim diameter using the data plotted in Figs. 9a, 10a, and 12a, against the scaling proposed[42]. As can be seen from the plot, all the curves collapse into a straight line, with a gradient, ϑ=1.23, which was obtained from averaging the gradient of the lines by least-square method. Hence, the new scaling relationship obtained becomes:

$$\frac{d_{crown}}{d} = 2\vartheta\left(\frac{2}{3}\right)^{1/4}\frac{v^{1/2}}{d^{1/4}h_N^{1/4}}(t-t_0)^{1/2}, \quad (2)$$

with ϑ=1.23. Equation (2) provides an approximation for the crown rim evolution over a significant fraction of its lifetime and reveals the changes brought about by the control of the liquid film. It does not contain viscosity and surface tension, however, since their effects only become important during the latter stages of the crown evolution.

E. Regional comparison

- **Effect of region of impact on number of secondary droplets**

In Fig. 14, we show the variation of ejected secondary droplets on the individual regions of impact on a controlled flowing film (i.e. capillary wave, flat film and wave hump) and an uncontrolled flowing

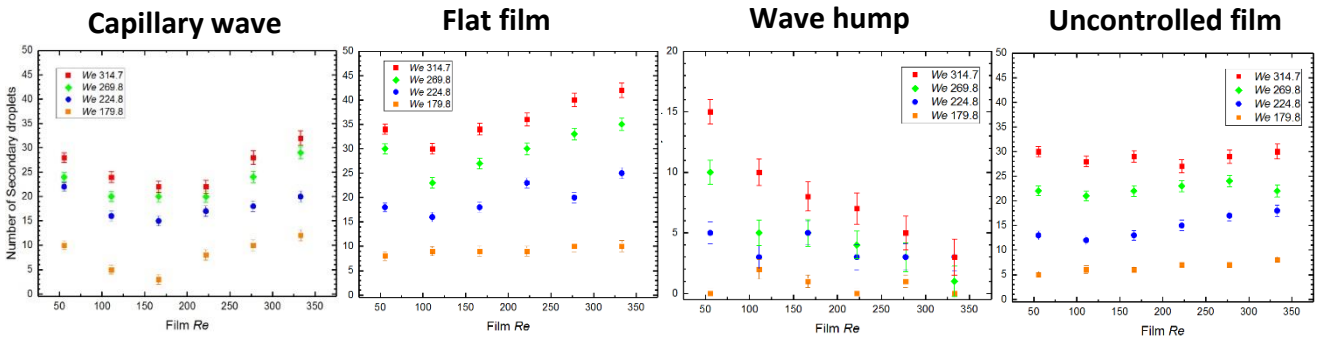

Fig. 14 Variation of the number of secondary droplets ejected from the crown rim in the different impact regions of a controlled film (viz 'capillary wave', 'flat film', and 'wave hump' regions, shown from left to right, respectively) contrasted against an uncontrolled film. The droplet size is 0.0033 mm corresponding to *Oh* = 0.0021, and the drop heights have been varied from 0.20-0.35, resulting in impact velocities within the range 1.981-2.621 m/s (corresponding to We_d = 179.8 – 314.7). The red rectangles depicts drop fall height of 0.35 m, the green diamonds 0.3 m, the blue circles 0.25 m, and the orange squares, 0.2 m, respectively.

film. The parameters used correspond to *Oh* = 0.0021, We_d = 179.8, 224.8, 269.8, and 314.7, and *Re* = 55.5 to 330. From the figure, an uneven trend of secondary droplet ejection is immediately observed with individual regions showing different trends. On the wave hump, it can be observed that only a few (or at times no) secondary drops are produced at low We_d, which is in contrast with the other regions of impact. However, we notice that with increasing We_d, there is a considerable ejection of droplets. These droplets are unlike those ejected on the flat film or capillary waves. They are rather large 'globules' which can be about 5-8 times the size of the drops in the other regions. Quantitatively, it was also observed that with increasing *Re*, the number of ejected secondary drop decreased (see Fig.14: column 3).

On the flat films, a different trend is observed. For the smallest We_d number examined (corresponding to a fall height of 0.2 m), the number of ejected secondary drop is essentially unaffected by the film flow rate. A range of 8-10 drops are observed generally. However, when the We_d is increased, the number of secondary drops also increases but the film flow rate effect now becomes noticeable. An undulation is noticed in the number of drops ejected but overall, the number increased (see Fig. 14: column 2). In comparison with the other regions of impact, the highest number of secondary drops were realised in the flat film region, which at times were as high as 40 drops. Hence, situations characterised by higher We_d values of the drop could not be examined as a result of this.

In the capillary wave region, the number of ejected drops follows a non-monotonic trend with respect to *Re* well but a monotonically-increasing one with We_d. The dip around Re values of 166.5 could be attributed to the competition between the tangential velocities of the drop and that of the film. At low We_d, values intermediate between those ejected on the flat film and wave hump regions are observed for the number of ejected secondary droplet, but an unpredictable undulation across the range of all film *Re* examined. With increase in the drop We_d, the number of secondary droplets ejected increases as well, but disproportionately. This trend observed in the number of ejected satellite drop is believed to occur as a result of the stochastic nature of the waves on the film surface

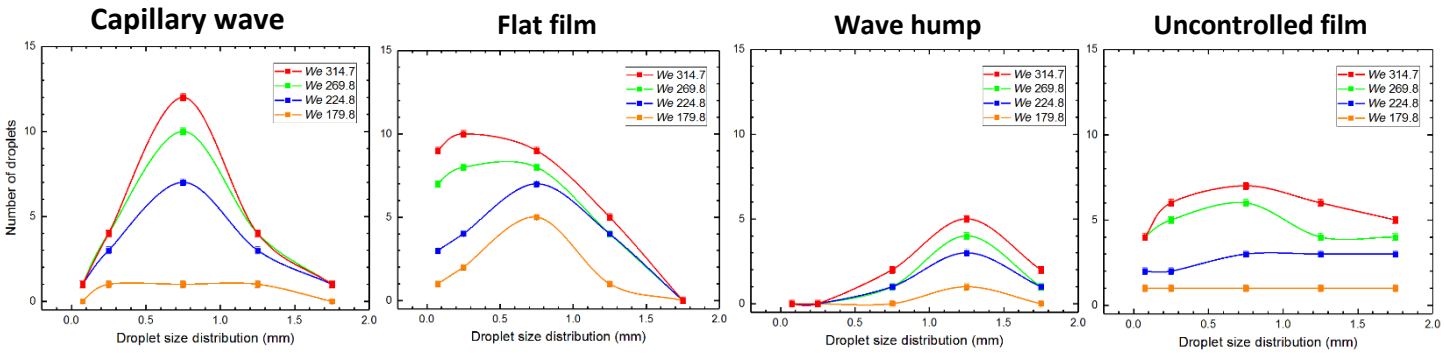

Fig. 15 Effect of impact region on size distribution of ejected secondary droplet on a controlled film contrasted against an uncontrolled film. The drop size is 0.0033 m while the film flow rate is 5 × 10^{-3} m^3/s corresponding to a film *Re* of 166.5 and drop *Oh* 0.0021. The drop's fall height are 0.2, 0.25, 0.3 and 0.35 m corresponding to We_d 179.8, 224.8, 269.8 and 314.7 respectively.

- **Effect of region of impact on size distribution of ejected secondary droplets**

The size distribution of the ejected secondary droplets in the different regions is shown in Fig. 15. The parameters used correspond to Oh = 0.0021, We_d = 179.8, 224.8, 269.8, and 314.7, and Re = 166.5. From the figure, it can be seen there is a clear difference in the size distribution of the secondary drops in these regions. On the capillary wave (Left panel; Fig 15), the shape of the distribution remains largely unaltered as the Weber number is increased but with a noticeable increase in the number of drops of range 0.5 to 1.0 mm. On the flat films, however, the size distribution is observed to vary from 0 to 2.0 mm, and a shift is observed towards the 0 to 0.5 mm sized drops as the Weber number is increased. This increase in the number of small drops ejected clearly differentiates the flat film region from the other regions. On the wave hump, as shown in the Fig 15 (panel 3), the size distribution shows that large drops in the range (1.0 to 2.0 mm) are ejected even for the smallest Weber number examined. In contrast to the above, the drop size distributions associated with an uncontrolled film do not exhibit a discernibly distinct shape owing to the stochastic nature of waves on such films.

IV. Conclusions

In this paper, we report the result of our experimental investigation of the effect of film control on droplet impact in the splashing regime. We have categorised the film surface on which the droplet impinges into three distinct regions of a typical solitary wave, namely the 'flat film', 'capillary wave', and 'wave hump' regions.[29,33,35] We have observe that on the wave hump of the solitary wave, fewer secondary droplets are ejected in comparison with those from the capillary, and flat film regions. The largest number of secondary droplets, however, are ejected from the flat film region due to the confinement offered by the substrate. The crown structure is also more regular on the wave hump and different from those observed to form in the other regions of impact. It is also larger and longer-lasting than the crowns associated with the capillary wave, and flat film regions. The distinctive features of this region (increased liquid mass, flow recirculation and usual velocity profile) are believed to be the main causes of these observed phenomena.

We have also observed that with increasing the film Reynolds number, Re, at constant drop Weber number, We_d, results in a change in the direction beyond which the crown of the wave hump faces, which is believed to be as a result of the competition between the inertia of the drop and the film. On the flat film, however, the crown tilt angle increases with Re while the crown on the capillary wave exhibits the opposite trend due to a flow reversal occurring here. The crown diameter is also weakly-dependent on Re but is a strong function of We_d as well as the drop size, characterised by the Ohnesorge number. Future work will involve the numerical simulation of the phenomena observed in the present paper.

Conflicts of interest

There are no conflicts of interest to declare.

Acknowledgements

We acknowledge the financial support of the Petroleum Technology Development Fund (PTDF, Nigeria) as well as the Engineering and Physical Sciences Research Council, UK, through the Programme Grant MEMPHIS (grant number EP/K003976/1).

References

1. A. L. Yarin, Drop impact dynamics: splashing, spreading, receding, bouncing…. *Annu. Rev. Fluid Mech.*. 2006, **38**, 159.
2. M. Rein, Phenomena of liquid drop impact on solid and liquid surfaces, *Fluid Dyn. Res.*, 1993, **12**, 61.
3. G. Liang and I. Mudawar, Review of mass and momentum interactions during drop impact on a liquid film, *International Journal of Heat and Mass Transfer*, 2016, **101**, 577.
4. D. B. van Dam and C. Le Clerc, Experimental study of the impact of an ink-jet printed droplet on a solid substrate, *Physics of Fluids*, 2004, **16**, 3403.
5. A. M. Worthington, A study of splashes. *Longmans, Green, and Company*; 1908.
6. H. E. Edgerton and J. R. Killian, Flash!: Seeing the unseen by ultra high-speed photography, *CT Branford Co.*, 1954.
7. C. Josserand and S. T. Thoroddsen, Drop impact on a solid surface, *Annual review of fluid mechanics*, 2016, **48**, 365.
8. J. M. Kolinski, L. Mahadevan and S. M. Rubinstein, Lift-off instability during the impact of a drop on a solid surface. *Physical review letters*, 2014, **112**, 134501.
9. P. V. Hobbs and T. Osheroff, Splashing of drops on shallow liquids, *Science*, 1967, **158**, 1184.
10. P. Adomeit and U. Renz, Hydrodynamics of three-dimensional waves in laminar falling films, *International journal of multiphase flow*, 2000, **26**, 1183.
11. F. Blanchette and T. P. Bigioni, Dynamics of drop coalescence at fluid interfaces, *Journal of Fluid Mechanics*, 2009, **620**, 333.
12. A. B. Wang and C. C. Chen, Splashing impact of a single drop onto very thin liquid films, *Physics of fluids*, 2000, **12**, 2155.
13. Z. Che, A. Deygas and O. K. Matar, Impact of droplets on inclined flowing liquid films, *Physical Review E.*, 2015, **92**, 023032.
14. S. K. Alghoul, C. N. Eastwick and D. B. Hann, Normal droplet impact on horizontal moving films: an investigation of impact behaviour and regimes, *Experiments in fluids*, 2011, **50**, 1305.
15. K. L. Pan and C. K. Law, Dynamics of droplet–film collision, *Journal of fluid mechanics*, 2007, **587**, 1.
16. F. Blanchette and T. P. Bigioni, Partial coalescence of drops at liquid interfaces, *Nature Physics*, 2006, **2**, 254.
17. T. Gilet, K. Mulleners, J. P. Lecomte, N. Vandewalle and S. Dorbolo, Critical parameters for the partial coalescence of a droplet, *Physical Review E*, 2007, **75**, 036303.
18. S. T. Thoroddsen and K. Takehara, The coalescence cascade of a drop, *Physics of Fluids*, 2000, **12**, 1265.

19. G. Agbaglah and R. D. Deegan, Growth and instability of the liquid rim in the crown splash regime, *Journal of Fluid Mechanics*, 2014, **752**, 485.
20. S. Mukherjee and J. Abraham, Crown behavior in drop impact on wet wall, *Physics of fluids*, 2007, **19**, 052103.
21. C. Josserand and S. Zaleski, Droplet splashing on a thin liquid film, *Physics of fluids*, 2003, **15**, 1650.
22. S. T. Thoroddsen, K. Takehara and T. G. Etoh, Micro-splashing by drop impacts, *Journal of Fluid Mechanics,* 2012, **706**, 560.
23. G. E. Cossali, A. Coghe and M. Marengo, The impact of a single drop on a wetted solid surface, *Experiments in fluids*, 1997, **22**, 463.
24. A. L. Yarin and D. A. Weiss, Impact of drops on solid surfaces: self-similar capillary waves, and splashing as a new type of kinematic discontinuity, *Journal of Fluid Mechanics*, 1995, **283**, 141.
25. D. Gueyffier, *Etude de l'impact de gouttes sur un film liquide mince: développement de la corolle et formation de projection* (Doctoral dissertation, Paris 6).
26. J. C. Bird, S. S. Tsai and H. A. Stone, Inclined to splash: triggering and inhibiting a splash with tangential velocity, *New Journal of Physics,* 2009, **11**, 063017.
27. M. M. Driscoll and S. R. Nagel, Ultrafast interference imaging of air in splashing dynamics, *Physical review letters*, 2011, **107**, 154502.
28. M. J. Thoraval, K. Takehara, T. G. Etoh and S. T. Thoroddsen, Drop impact entrapment of bubble rings*, Journal of Fluid Mechanics*, 2013, **724**, 234.
29. R. V. Craster and O. K. Matar, Dynamics and stability of thin liquid films, *Reviews of modern physics*, 2009, **81**, 1131.
30. P. N. Yoshimura, T. Nosoko and T. Nagata, Enhancement of mass transfer into a falling laminar liquid film by two-dimensional surface waves—some experimental observations and modelling, *Chemical Engineering Science*, 1996, **51**, 1231.
31. H. H. Chang and E. A. Demekhin, Complex wave dynamics on thin films, *Elsevier*, 2002.
32. S. V. Alekseenko, V. E. Nakoryakov and B. G. Pokusaev, Wave flow of liquid films, *New York: Begell House*, 1994.
33. J. Liu and J. P. Gollub, Solitary wave dynamics of film flows. *Physics of Fluids*, 1994, **6**, 1702.
34. T. B. Benjamin, Wave formation in laminar flow down an inclined plane, *Journal of Fluid Mechanics,* 1957, **2**, 554.
35. S. Kalliadasis, C. Ruyer-Quil, B. Scheid and M. G. Velarde, Falling liquid films. *Springer Science & Business Media*, 2011.
36. A. Charogiannis, F. Denner, B. G. van Wachem, S. Kalliadasis and C. N. Markides, Detailed hydrodynamic characterization of harmonically excited falling-film flows: A combined experimental and computational study. *Physical Review Fluids*, *2017,* **1**, 2
37. I. Adebayo, Z. Xie, Z. Che, and O. K. Matar, Doubly excited pulse waves on thin liquid films flowing down an inclined plane: An experimental and numerical study. *Physical Review E*, 2017, **96**, 013118.
38. M. Rieber and A. Frohn, A numerical study on the mechanism of splashing, *International Journal of Heat and Fluid Flow,* 1999, **20**, 455.
39. I. V. Roisman and C. Tropea, Impact of a drop onto a wetted wall: description of crown formation and propagation*, Journal of Fluid Mechanics,* 2002, **472**, 373.
40. A. J. Mitchell, D. Hann, K. Simmons, Experimental Investigation Into Crater Morphology for Droplets Impinging on a Moving Film. *Turbomachinery Technical Conference and Exposition,* 2017 (pp. V02DT48A006-V02DT48A006).
41. D.B. Hann, A.V. Cherdantsev, A. Mitchell, I.N. McCarthy, B.N. Hewakandamby, K. Simmons. A study of droplet impact on static films using the BB-LIF technique. *Experiments in Fluids*. 2016, **4,** 46.
42. G. E. Cossali, M. Marengo, A. Coghe and S. Zhdanov, The role of time in single drop splash on thin film, *Experiments in Fluids*, 2004, **36**, 888.
43. A. L. Yarin and D. A. Weiss, *J. Fluid Mech.*, 1995, **283**, 141–173.